Long *et al. Microstructures* 2024;4:2024011
DOI: 10.20517/microstructures.2023.58

Microstructures

Review

Open Access

Check for updates

La(Fe,Si/Al)$_{13}$-based materials with exceptional magnetic functionalities: a review

Feixiang Long[1], Yuzhu Song[1], Jun Chen[1,2]

[1]Department of Physical Chemistry, Beijing Advanced Innovation Center for Materials Genome Engineering, University of Science and Technology Beijing, Beijing 100083, China.
[2]Hainan University, Haikou 570228, Hainan, China.

Correspondence to: Prof. Yuzhu Song, Department of Physical Chemistry, University of Science and Technology Beijing, No. 30 Xueyuan Road, Haidian District, Beijing 100083, China. E-mail: yuzhusong@ustb.edu.cn; Prof. Jun Chen, Department of Physical Chemistry, University of Science and Technology Beijing, No. 30 Xueyuan Road, Haidian District, Beijing 100083, China. E-mail: junchen@ustb.edu.cn

How to cite this article: Long F, Song Y, Chen J. La(Fe,Si/Al)$_{13}$-based materials with exceptional magnetic functionalities: a review. *Microstructures* 2024;4:2024011. https://dx.doi.org/10.20517/microstructures.2023.58

Received: 17 Oct 2023 **First Decision:** 15 Dec 2023 **Revised:** 28 Dec 2023 **Accepted:** 19 Feb 2024 **Published:** 26 Feb 2024

Academic Editor: Danmin Liu **Copy Editor:** Fangling Lan **Production Editor:** Fangling Lan

Abstract

The field of magnetic functional materials continues to garner significant attention due to its research and diverse applications, such as magnetic storage and spintronics. Among these, La(Fe,Si/Al)$_{13}$-based materials exhibit abundant magnetic properties and emerge as highly captivating subjects with immense potential. This review provides an overview of the diverse magnetic structures and itinerant electron metamagnetic transition observed in La(Fe,Si/Al)$_{13}$-based materials. The transformation of different magnetic configurations elicits the phenomena such as negative thermal expansion, magnetostriction, magnetocaloric effect, and barocaloric effect. In addition, the pivotal role of spin and lattice coupling in these phenomena is revealed. The magnetic functionalities of La(Fe,Si/Al)$_{13}$-based materials can be controlled through adjustments of magnetic exchange interactions. Key methods, including chemical substitution, external field application, and interstitial atom insertion, enable precise modulation of these functionalities. This review not only provides valuable insights into the design and development of magnetic functional materials but also offers significant contributions to our understanding of the underlying mechanisms governing their magnetic behaviors.

Keywords: La(Fe,Si/Al)$_{13}$, spin-lattice coupling, magnetic functionalities, magnetic structures

INTRODUCTION

The discovery of magnetism dates back as far as the sixth century B.C. In ancient times, compasses made of magnetic materials were used for navigation. The magnetism of a material comes from the spin and orbital magnetic moments of the electrons outside the nucleus in an atom. Since electrons in 3*d* orbitals cannot exhibit orbital magnetic moments due to the orbital quenching effect, the magnetism is mainly contributed by the spin magnetic moments of the electrons. The magnetism of the 4f-rare earth elements, especially the heavy rare earth elements, is contributed by spin and orbital magnetic moments. Transition metal and rare earth elements constitute a variety of intermetallic compounds, exhibiting abundant magnetic properties and possessing crucial applications across various fields in contemporary society. For example, hard disk drives made of hard magnetic materials can store data stably and are widely used in computers and information technology. The magnetovolume effect (MVE) enables magnetic materials to exhibit zero thermal expansion (ZTE) or negative thermal expansion (NTE) phenomena[1,2]. The entropy change that accompanies the magnetic phase transition process lays the groundwork for the development of solid-state refrigeration materials[3-5]. Magnetic or hydrostatic refrigeration devices can be fabricated using magnetic fields or hydrostatic pressure to drive phase transitions in magnetic materials. In addition, spintronics based on magnetic materials offers excellent potential for the development of new electronic devices and information processing technologies[6,7].

Among a series of intermetallic compounds composed of transition and rare earth elements, $La(Fe,Si/Al)_{13}$ is a class of compounds with excellent magnetic properties first reported by Palstra *et al.* in 1983[8]. $La(Fe,Si/Al)_{13}$ compounds exhibit an itinerant-electron metamagnetic (IEM) transition induced by temperature, magnetic field, or hydrostatic pressure. The origin of the IEM transition is associated with a special 3*d* band structure related to a sharp peak of the density of states (DOS) just below the Fermi level[9,10]. Due to the coupling of spin and lattice, the IEM transition in $La(Fe,Si/Al)_{13}$ under different fields is accompanied by many potential physical effects. For instance, during the temperature change process, the NTE of the $La(Fe,Si/Al)_{13}$-based materials can compensate for the expansion of the positive thermal expansion materials, resulting in ZTE materials. The magnetostriction can be induced by IEM transition when loading a magnetic field. Furthermore, entropy changes can also be achieved when loading a magnetic field or hydrostatic pressure. The importance of $La(Fe,Si/Al)_{13}$ is self-evident in the field of magnetic functional materials.

In this article, we review the research progress on $La(Fe,Si/Al)_{13}$-based materials, focusing primarily on their crystal structures, magnetic properties, microscopic magnetic structures, and related functionalities. The magnetic and crystal structures, magnetostriction, NTE, magnetocaloric effect (MCE), and barocaloric effect (BCE) are discussed in detail [Figure 1]. Then, the correlation between these properties and magnetic phase transition is revealed. Meanwhile, the importance of IEM transition and spin-lattice coupling under different fields in magnetic functionalities and how to control the functionalities by adjusting the magnetic transition are summarized. Finally, the outstanding properties of $La(Fe,Si/Al)_{13}$-based materials and their excellent application value are concluded. This review is expected to steer the practical application of $LaFe_{13}$-based materials and contribute to the design of magnetic functional materials more broadly.

STRUCTURAL AND MAGNETIC FEATURES OF $LAFE_{13}$-BASED MATERIALS

$LaFe_{13}$-based materials are usually synthesized by arc melting or induction melting. The synthesized samples must be placed in quartz tubes under vacuum, annealed at 1,323 K for at least five days, and quenched in ice water. To shorten the synthesis time, some other methods have been explored, such as Spark Plasma Sintering (SPS) and combining high-energy ball milling with a subsequent short annealing treatment[11]. The $LaFe_{13}$-based materials are cubic $NaZn_{13}$-type structures with a space group of Fm-3c [Figure 2A]. There are

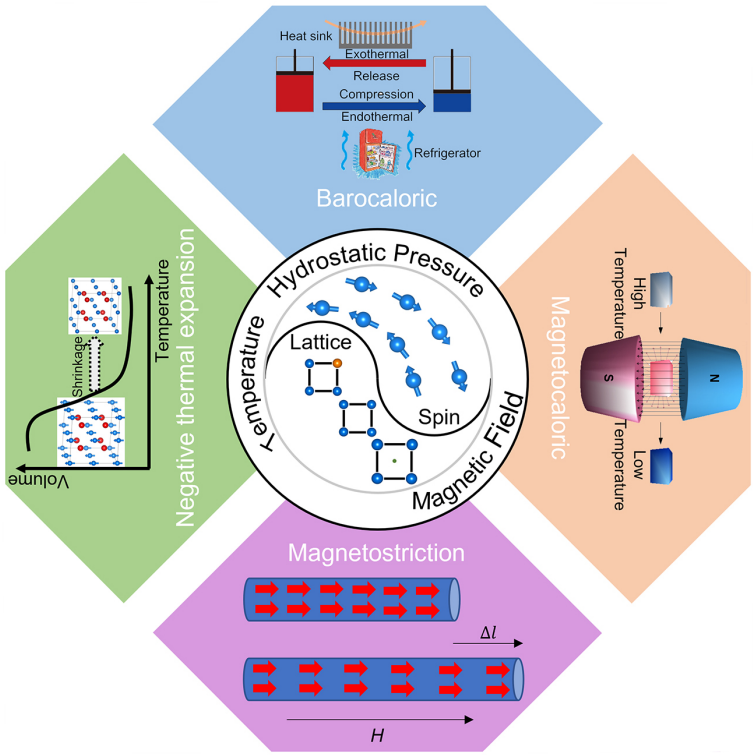

Figure 1. Exceptional magnetic properties (NTE, MCE, BCE, and magnetostriction) induced by spin-lattice coupling.

112 atoms in the unit cell. The Wyckoff positions for Fe1 and Fe2 are 8b and 96i, and the Wyckoff position for La is 8a. La and Fe1 atoms form CsCl-type structures. Each Fe1 atom is located at the center of an icosahedron composed of twelve Fe2 atoms, and there are one Fe1 and nine Fe2 atoms at the nearest-neighbor position of each Fe2 atom. The binary compound $LaFe_{13}$ does not exist because the enthalpy of generation between La and Fe atoms is positive. However, the chemical affinity between La and Si or Al is robust. Replacing a portion of the Fe atoms with Si or Al atoms stabilizes the $LaFe_{13}$-based materials in a $NaZn_{13}$-type structure, with the Si or Al atoms and the Fe2 atoms occupying the 96i positions together. The $NaZn_{13}$ phase forms via the peritectic reaction of liquid La and Fe with solid $LaFe_2Si_2$[11]. Under the condition of sufficient annealing time, excessive amounts of Fe and La can give rise to the formation of a second phase of Fe and LaFeSi in $LaFe_{13}$-based materials, respectively [Figure 2B][12]. Although an excess of Si or Al elements would typically not produce a second phase in $LaFe_{13}$-based materials, there exists a limit beyond which the structural and magnetic properties may be negatively affected. For $LaFe_{13-x}Si_x$, it will be stabilized in the cubic phase and ferromagnetic (FM) state when $1.3 \leq x \leq 2.6$ [Figure 2C], and a further increase in the Si content will form a different tetragonal $Ce_2Ni_{17}Si_9$-type phase[13,14]. For $LaFe_{13-x}Al_x$, the compounds are stabilized in the cubic phase when $1.04 \leq x \leq 7.02$[15]. The system exhibits an antiferromagnetic (AFM) state when $1.04 \leq x < 1.7$ and an FM state when $1.7 \leq x \leq 4.9$ [Figure 2D]. Figure 2E demonstrates a magnetic phase diagram of $LaFe_{11.4}Al_{1.6-x}Si_x$ ($0 \leq x \leq 1.6$). $LaFe_{11.4}Al_{1.6-x}Si_x$ materials are AFM when the Si content $x \leq 0.2$. The Neel temperature T_N decreases as the Si content increases. FM clusters appear when Si content $x = 0.22$. $LaFe_{11.4}Al_{1.6-x}Si_x$ materials undergo an FM-AFM transition at T_0 and an AFM-paramagnetic (PM) transition at Curie temperature (T_C) with T_N when $0.25 \leq x \leq 0.40$. With further increasing Si content $0.50 \leq x \leq 1.60$, only an FM-PM transition occurs at T_C which increases with the higher Si content in the compound. The AFM exchange interactions between Fe atoms in the AFM state of $LaFe_{13-x}Al_x$ are relatively weak, so it is easily affected by external fields or substitutions. In addition to FM [Figure 2F] and AFM [Figure 2G] structures, the canting magnetic structure is observed in $LaFe_{11.5}Al_{1.5}$ under the influence of an external

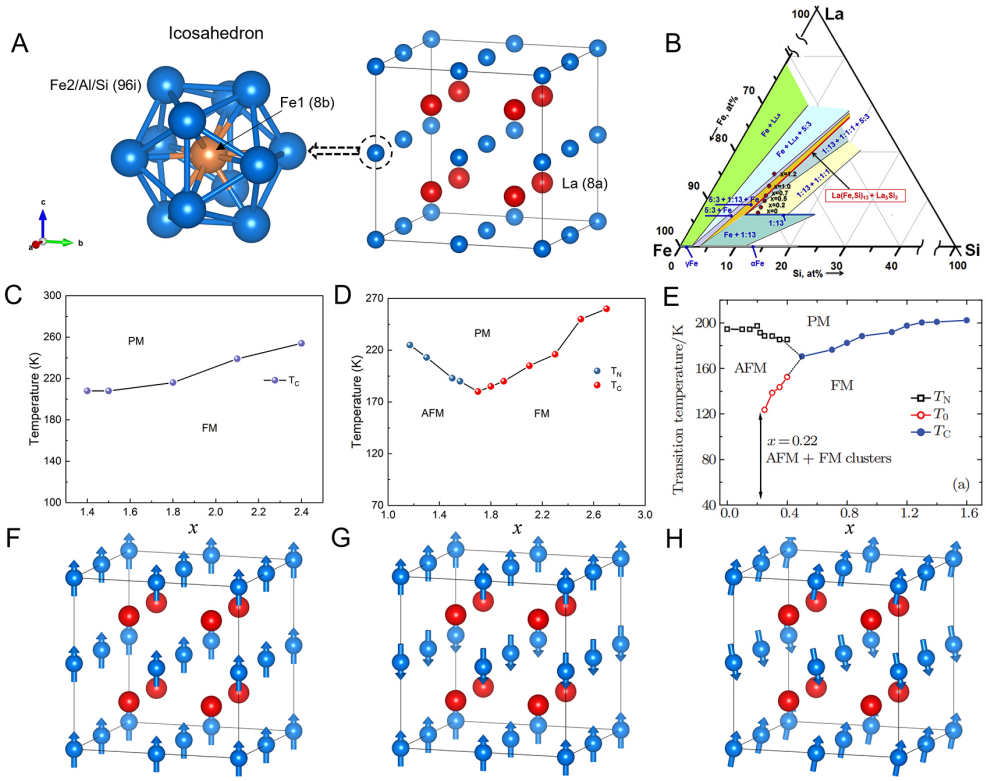

Figure 2. (A) Structure schematic of La(Fe,Si/Al)$_{13}$-based materials. (B) La-Fe-Si partial isothermal section at 1,373 K[12]. (C-E) Magnetic phase diagrams for $LaFe_{13-x}Si_x$, $LaFe_{13-x}Al_x$, and $LaFe_{11.4}Al_{1.6-x}Si_x$[17]. (F-H) Magnetic structures for FM, AFM, and canting AFM states. (B) is reproduced with the permission of Ref.[12] Copyright 2016, Elsevier. (E) is reproduced with the permission of Ref.[17] Copyright 2013, Editorial Office of Chinese Physics B.

magnetic field using variable magnetic field neutron powder diffraction experiments [Figure 2H][16]. On the basis of these results, it can be concluded that the substitution of Si atoms, which possess a smaller radius compared to Al atoms, leads to the emergence of an FM state in $LaFe_{13}$-based materials. Conversely, substituting a small quantity of Al atoms for Fe atoms results in an AFM state, while increasing the quantity of Al content causes a transition to an FM state. When Al and Si are simultaneously introduced to replace Fe atoms, the magnetic phase diagram of $LaFe_{13}$-based materials becomes more complicated, showcasing the coexistence of both FM and AFM states in a narrow region [Figure 2E][17].

Due to the coupling of spin and lattice, several methods can be used to modulate the magnetic transition in $LaFe_{13}$-based materials. Subjecting the material to hydrostatic pressure results in lattice compression, which causes a reduction in the T_C. New magnetic atoms can be introduced into the La(Fe,Si/Al)$_{13}$-based materials by replacing Fe with other transition metal atoms. Chemical pressures can be exerted on the lattice of the materials by adjusting the content of Si or Al atoms and inserting interstitial atoms. The magnetic transition can be effectively controlled through various factors, such as their lattice constants, bonding between atoms, the position of the Fermi energy levels, electron concentration, and magnetic exchange interactions. In the case of $LaFe_{13-x}Si_x$, the T_C of the materials decreases when loading hydrostatic pressures[18]. This phenomenon indicates that the decreased atomic distance directly weakens the magnetic exchange interactions and leads to a lower T_C in $LaFe_{13-x}Si_x$. On the other hand, hydrogenation can be used to insert hydrogen (H) atoms into the materials[19]. Neutron powder diffraction experiments are performed to obtain the interstitial site of H atoms and their influence on crystal structure. The interstitial H atoms are located on the 48f site, and the unit cell parameter increases linearly with hydrogen content[20,21]. The T_C of the material gradually increases

as the number of H atoms inserted rises. The impact of hydrostatic pressure and H atoms on the material reveals that expanded atomic distance can lead to higher T_C, while contracted atomic distance can reduce the T_C of the material. However, the situation changes when more Si atoms are introduced, as it leads to a decrease in atomic distance and a corresponding increase in T_C[22]. Thus, the substitution of more Si atoms changes the electronic structure and magnetic exchange interactions. When using transition metal atoms with smaller radii, such as Co, Ni, and Cu, to replace Fe, it has a similar effect in increasing the T_C[23,24]. This is caused by the changes of magnetic exchange interaction and the electronic structure. Furthermore, it transforms a first-order magnetic phase transition to a second-order magnetic phase transition when atoms such as Co, Ni, and Cu replace Fe atoms at a concentration of more than 1.6 in $LaFe_{13-x}Si_x$[24]. In addition, using transition metals with larger radii, such as Cr and Mn, to replace Fe has the opposite effect and can lead to a lower T_C[25]. Therefore, the T_C is not solely dependent on atomic distance but also on magnetic exchange interactions between different atoms and electronic structure of the $LaFe_{13}$-based materials; the specific theoretical explanation of these observations in different regulatory methods is temporarily ambiguous.

NOVEL FUNCTIONALITIES OF $LAFE_{13}$-BASED MATERIALS

There is a remarkable IEM transition in $LaFe_{13}$-based materials, which can change between PM, FM, and AFM states driven by external fields[26]. Therefore, $LaFe_{13}$-based materials can exhibit many novel phenomena under the effect of different external fields. Here, we focus on the physical effects of $LaFe_{13}$-based materials, including NTE, magnetostriction, MCE, and BCE.

Excellent negative thermal expansion of $LaFe_{13}$-based materials

NTE is an interesting and unconventional thermal expansion behavior resulting from interactions of lattice, electron, and phonon. Magnetic NTE materials are an important part of NTE materials[1]. The study of magnetic NTE materials can be traced back to the discovery of ZTE of $Fe_{65}Ni_{35}$ Invar alloy in 1896[27]. The ZTE nature of magnetic NTE materials results from the MVE during the transition from magnetic order to magnetic disorder structure[28,29]. The $LaFe_{13}$-based materials change from an FM state to a PM state at high temperatures. These magnetic transition processes are strongly coupled to the lattice and accompanied by strong MVE, which manifests giant NTE phenomena[30].

$LaFe_{13}$-based materials exhibit giant NTE near the magnetic transition temperature. In $La(Fe,Si)_{13}$, increasing the Si content results in a change of electronic structure, which leads to an increase in magnetic exchange interaction, resulting in a rise in T_C. As shown in Figure 3A, the temperature range of the NTE broadens but the strength weakens when the substitution of Si for Fe increases in $LaFe_{13-x}Si_x$. In $LaFe_{11.5}Si_{1.5}$, the coefficient of thermal expansion is α_l = -50.1 × 10^{-6} K^{-1} from 170 to 240 K, and in $LaFe_{10.6}Si_{2.4}$, the coefficient of thermal expansion is α_l = -11.2 × 10^{-6} K^{-1} from 160 to 270 K. In addition, Huang *et al.* found a near-zero expansion phenomenon in the range of 15-150 K[31]. The NTE phenomenon is weaker in $LaFe_{13-x}Al_x$ due to its MVE being relatively weak, resulting from its weak magnetic properties and the IEM transition. As shown in Figure 3B, the coefficients of thermal expansion are α_l = -10.47 × 10^{-6} K^{-1} for $LaFe_{11.2}Al_{1.8}$ and -4.64 × 10^{-6} K^{-1} for $LaFe_{10.7}Al_{2.3}$ from 100 to 225 K[32]. Despite the excellent NTE properties in both $LaFe_{13-x}Si_x$ and $LaFe_{13-x}Al_x$, their NTE temperature is relatively low, making it difficult to meet the requirements of room temperature use. Interestingly, the chemical substitution of Fe with Co can increase the NTE temperature range by adjusting the lattice, electron concentration, and band structure, as shown in Figure 3C and D[23,31]. $LaFe_{10.5}Co_{1.0}Si_{1.5}$ exhibits a linear coefficient of thermal expansion of α_l = -26.1 × 10^{-6} K^{-1} within the temperature range of 240-350 K, which covers the room temperature and has a temperature window of 110 K. Substitution of Fe with Co increases the NTE temperature and enhances the NTE for $LaFe_{11.4-x}Co_xAl_{1.6}$. As shown in Figure 3D, the linear thermal expansion coefficients are α_l = -16.73 × 10^{-6} K^{-1}

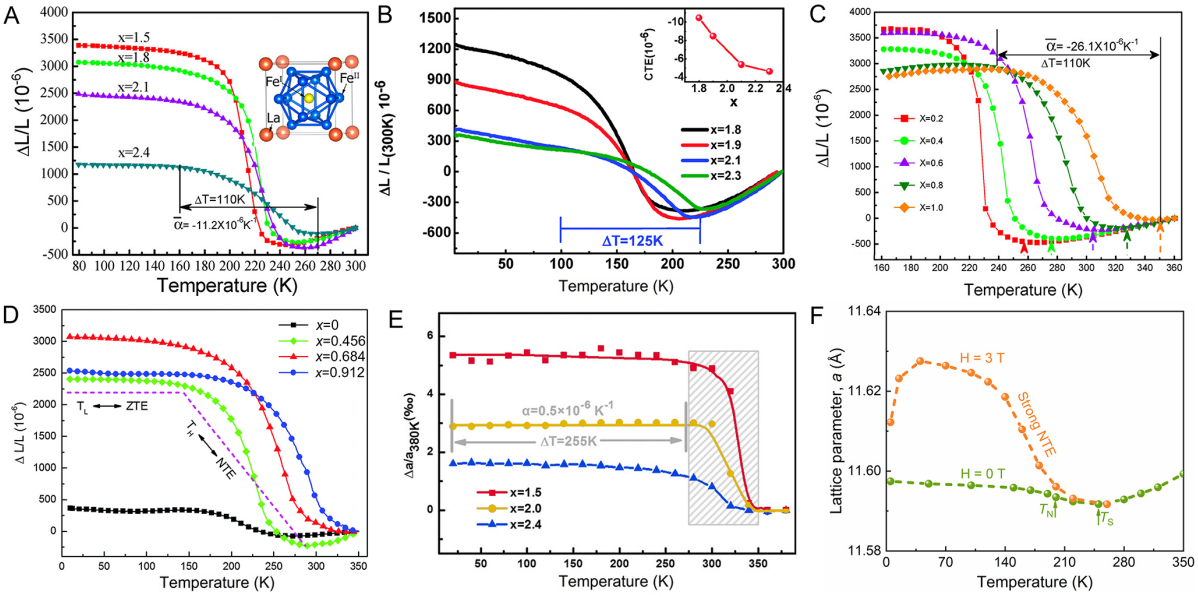

Figure 3. Temperature dependence of linear thermal expansion $\Delta L/L_0$ of (A) $LaFe_{13-x}Si_x$[31], (B) $LaFe_{13-x}Al_x$[32], (C) $LaFe_{11.5-x}Co_xSi_{1.5}$[31], (D) $LaFe_{11.4-x}Co_xAl_{1.6}$[23], (E) $LaFe_{13-x}Si_x$ hydrides[19]. (F) Temperature dependence of the lattice parameter in $LaFe_{11.5}Al_{1.5}$ at H = 0 T (green line) and H = 3 T (orange line)[16]. (A and C) are reproduced with the permission of Ref.[31] Copyright 2013, American Chemical Society. (B) is reproduced with the permission of Ref.[32] Copyright 2015, Royal Society of Chemistry. (D) is reproduced with the permission of Ref.[23] Copyright 2016, Royal Society of Chemistry. (E) is reproduced with the permission of Ref.[19] Copyright 2017, John&Wiley Sons. (F) is reproduced with the permission of Ref.[16] Copyright 2020, American Chemical Society.

from 138 to 290 K for x = 0.456 and α_l = -12.96 × 10^{-6} K^{-1} from 160 to 350 K for x = 0.912. Generally, the NTE occurs near the FM-PM or AFM-PM transitions in magnetic NTE materials, which implies that the NTE is strongly related to the magnetic order transition. The MVE resulting from the IEM transition causes strong NTE phenomena in $La(Fe,Si/Al)_{13}$-based materials. Replacing Fe with Co increases the magnetic transition temperature by changing the electron distribution near the Fermi surface and enhancing the magnetic exchange interactions. The AFM-PM transition that occurs in $LaFe_{11.4}Al_{1.6}$ leads to the emergence of NTE, and the substitution of Co for Fe is not only able to increase the magnetic transition temperature but also change the AFM state to the FM state, which leads to the enhancement of the IEM. As a result, an enhanced NTE that expands to room temperature can be obtained in $La(Fe,Si/Al)_{13}$-based materials.

In addition to the chemical substitution, hydrogenation can be employed to control the NTE of $LaFe_{13}$-based materials. Li *et al.* achieved the hydrogenation of $La(Fe,Si)_{13}$ by electrolysis and investigated the effect of H insertion on the NTE [Figure 3E][19]. The H-inserted $La(Fe,Si)_{13}$ maintains the $NaZn_{13}$-type cubic structure. The hydrogenation causes a significant change in its thermal expansion properties compared to $La(Fe,Si)_{13}$. The NTE temperature range of hydrogenated $La(Fe,Si)_{13}$ moved from 175-250 to 275-350 K, which covers the room temperature. At the same time, the strength of NTE is weakened. Hydrogenated $La(Fe,Si)_{13}$ exhibits excellent ZTE properties in the low-temperature range. The average thermal expansion coefficient of $LaFe_{11}Si_2$ is -9.2 × 10^{-6} K^{-1} from 15 to 175 K, whereas the average thermal expansion coefficient of hydrogenated $LaFe_{11}Si_2$ is 0.5 × 10^{-6} K^{-1} over a wider temperature range from 20 to 275 K. The insertion of H atoms into the lattice appears as a negative pressure effect and leads to an expansion of the interatomic distance, and the T_C increases with the insertion of more H atoms. Therefore, the magnetic transition from an ordered to a disordered state in H-inserted $La(Fe,Si)_{13}$ characterized by a correspondingly higher amount of thermal energy is required. The concurrent attenuation of the spin fluctuation results in a lessened MVE, ultimately leading to the manifestation of a ZTE phase in hydrides at lower temperatures. Song *et al.*

investigated the NTE of $LaFe_{11.5}Al_{1.5}$ through in situ magnetic field neutron powder diffraction. Remarkably, a giant NTE was observed at a magnetic field strength of 3 T [Figure 3F][16]. The neutron powder diffraction experiments reveal that under the influence of the magnetic field, the canting spin in $LaFe_{11.5}Al_{1.5}$ rotates in the direction of the magnetic field. The FM components gradually increase while the AFM components are gradually reduced, accompanied by a volume expansion. However, the volume of the PM state remains unchanged. This magnetic-field-induced effect is found to significantly enhance the NTE behavior in $LaFe_{11.5}Al_{1.5}$, shedding light on the intricate interplay between magnetic field, crystal structure, and thermal expansion in this material system.

The ability of NTE materials to control the thermal expansion coefficient of materials has attracted extensive research interest in the past few decades. $La(Fe,Si/Al)_{13}$-based materials demonstrate giant NTE over a wide temperature range which can be modulated via chemical substitution, external field application, and interstitial atom insertion. These approaches realize the control of the coupling of spin and lattice. Future work may focus on the enhancement of NTE and exploring the fabrication of composite materials to achieve ZTE, presenting exciting prospects for the development of advanced magnetic functional materials with diverse thermal properties. Recently, Pang *et al.* prepared composite materials with five different components of $La(Fe,Co,Si)_{13}$ and Cu[33]. This composite material exhibits high thermal conductivity and ZTE over a wide temperature range, which shows great application prospects for $LaFe_{13}$-based materials.

Magnetostriction in $LaFe_{13}$-based materials

The magnetostriction effect, an intriguing phenomenon observed in certain magnetic materials, refers to the phenomenon in which the dimensions of the material undergo changes upon the application of a magnetic field. The underlying mechanism of magnetostriction involves the modification of magnetic moments and spin in crystals and their consequential coupling with the lattice in the presence of an external magnetic field. This phenomenon holds significant relevance in several research areas, including materials science and electronic devices[34-36]. Generally, magnetic NTE can be regarded as spontaneous volume magnetostriction driven by temperature. Therefore, the giant NTE in $La(Fe,Si/Al)_{13}$-based materials indicates large volume differences between different magnetic states, which means that $La(Fe,Si/Al)_{13}$-based materials can also exhibit giant magnetostriction under magnetic fields. Moreover, $La(Fe,Si/Al)_{13}$-based materials are characterized by remarkable IEM transitions in response to an external magnetic field, which establishes an excellent foundation for their exceptional magnetostriction effect. Specifically, $LaFe_{11.4}Si_{1.6}$ manifests a distinctly discernable impact of the external magnetic field upon the magnetic moments and spin fluctuations at temperatures marginally greater than T_C, potentiating a giant magnetostriction effect. Moreover, $LaFe_{13-x}Al_x$ ($1.04 \leq x \leq 1.8$) affords an unusual magnetostriction owing to its more unstable AFM state, which can undergo an IEM transition upon the application of an external magnetic field, subsequently transforming into an FM state.

Fujita *et al.* investigated the magnetostriction of $LaFe_{11.44}Si_{1.56}$, characterized by a T_C of 195 K [Figure 4A][37]. The application of a magnetic field of approximately 1 T at a temperature of 200 K causes $LaFe_{11.4}Si_{1.6}$ to transform from a PM state to an FM state. Significantly, magnetostriction along the magnetic field in $LaFe_{11.44}Si_{1.56}$ reaches a maximum at 0.5% under a magnetic field strength reaching 7 T, which is attributed to the radical alterations induced in the spin polarization and spin fluctuations of the material by the impact of an external magnetic field[37]. The impact of hydrogenation on the magnetostriction of this group of materials has also been investigated by Fujieda *et al.* [Figure 4B][38]. The insertion of 1 mol of H atoms into $LaFe_{11.44}Si_{1.56}$ results in an elevation of the T_C to 278 K. At the temperature range between 284 and 288 K, the application of an external magnetic field with a magnitude of 7 T prompts magnetostriction along the magnetic field exceeding 0.3%, corresponding to an estimated variation of unit cell volume of approximately 1%. Hydrogenation has been demonstrated to effectuate an elevation in the T_C of $LaFe_{11.44}Si_{1.56}$,

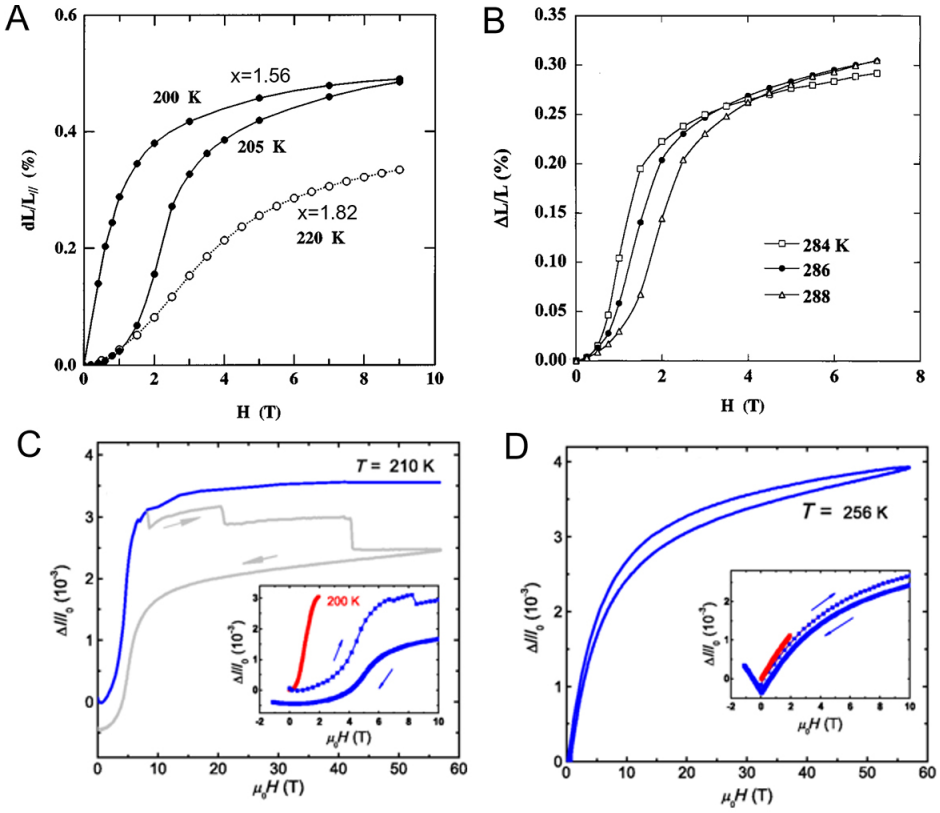

Figure 4. Magnetic-field dependence of the magnetostriction parallel to the magnetic field just above the Curie temperature for (A) $LaFe_{13-x}Si_x$ [37], (B) $LaFe_{11.44}Si_{1.56}H_1$ [38]. (C and D) Magnetostriction measured at 210 K for $LaFe_{11.74}Co_{0.13}Si_{1.13}$ and 256 K for $LaFe_{11.21}Co_{0.65}Si_{1.11}$. The insets display the pulsed-field data (blue line) together with the static-field data (red line)[39]. (A) is reproduced with the permission of Ref.[37] Copyright 1999, AIP Publishing. (B) is reproduced with the permission of Ref.[38] Copyright 2001, AIP Publishing. (C and D) are reproduced with the permission of Ref.[39] Copyright 2017, American Physical Society.

concomitantly facilitating the onset of IEM in the presence of an applied magnetic field at near-ambient temperatures. Thus, magnetostriction in $LaFe_{11.44}Si_{1.56}$ can be modulated to near-ambient temperature by hydrogenation[38]. Due to the coupling of spin and lattice, magnetostriction in $La(Fe,Si)_{13}$ materials is further studied by substituting Fe atoms with Co and Mn atoms. $LaFe_{11.7}Co_{0.13}Si_{1.13}$ demonstrates a 0.35% magnetostriction along the magnetic field at 210 K under the action of a strong pulsed magnetic field, achieving saturation at approximately 15 T magnetic field strength. $LaFe_{11.21}Co_{0.85}Si_{1.11}$ exhibits a 0.4% magnetostriction along the magnetic field at 256 K, with further enhancement observed beyond a magnetic field of 55 T [Figure 4C and D][39]. Abdulkadirova *et al.* demonstrate that $LaFe_{11.1}Mn_{0.1}Co_{0.7}Si_{1.1}$ exhibits maximal magnetostriction at temperatures slightly above the T_C of 252 K, reaching 0.26% along the magnetic field with the application of a 12 T magnetic field[40]. Notably, the magnetostriction weakens at lower temperatures or with continued warming, indicating the sensitivity of spin polarization and spin fluctuations in magnetic materials to external magnetic fields. Therefore, the giant magnetostriction is only achieved upon experiencing IEM transitions [Figure 5A]. The substitution of Co and Mn atoms weakens magnetostriction compared to $La(Fe,Si)_{13}$, but the presence of Co atoms remarkably elevates the temperature range over which magnetostriction can occur, representing a crucial advancement in the control of magnetostriction within this class of materials.

In contrast to the behavior observed in $La(Fe,Si)_{13}$ materials, $LaFe_{13-x}Al_x$ ($1.04 \leq x \leq 1.7$) exhibits an IEM transition below the Neel temperature T_N in the presence of an external magnetic field. This transition leads

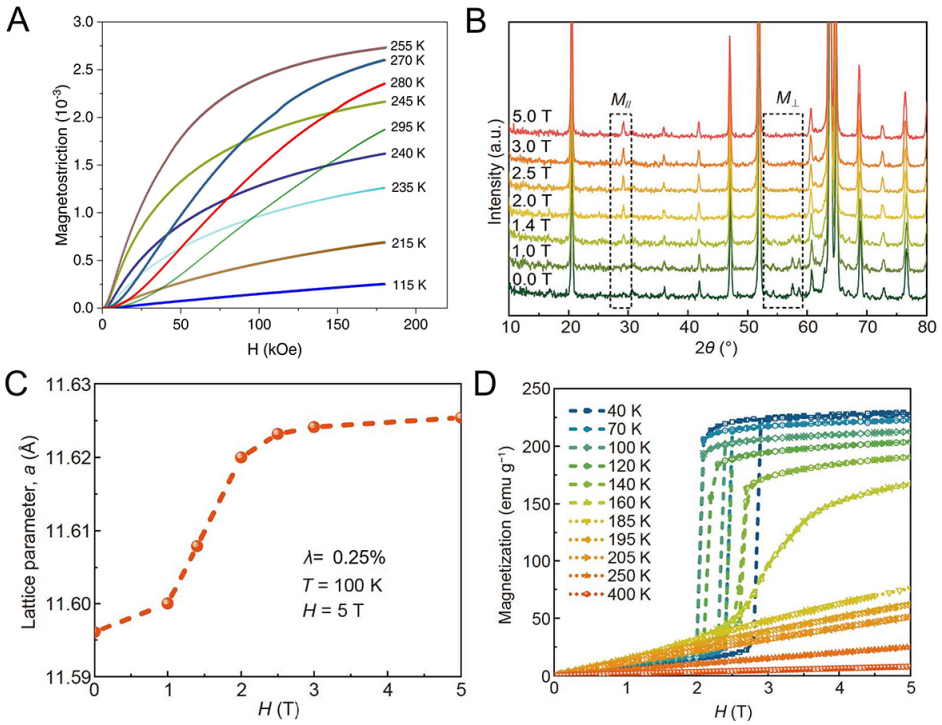

Figure 5. (A) Field and temperature dependences of the magnetostriction for $LaFe_{11.1}Mn_{0.1}Co_{0.7}Si_{1.1}$ [40]. (B) Magnetic-field dependence of neutron powder diffraction patterns of $LaFe_{11.5}Al_{1.5}$ at T = 100 K[15]. (C) Magnetic-field dependence of lattice parameter of $LaFe_{11.5}Al_{1.5}$ at H = 5 T[15]. (D) Isothermal magnetization (M-H) of $LaFe_{11.5}Al_{1.5}$ at selected temperatures[15]. (A) is reproduced with the permission of Ref.[40] Copyright 2022, Elsevier. (B-D) are reproduced with the permission of Ref.[15] Copyright 2021, Springer Nature.

to a transformation from an AFM state to an FM state, accompanied by magnetostriction estimated to be around 0.3% along the magnetic field. Song *et al.* revealed the origin of magnetostriction in $La(Fe,Al)_{13}$ for the first time by neutron powder diffraction experiments with in situ magnetic fields and temperature[15]. The neutron data reveal the exact canting AFM structure of $La(Fe,Al)_{13}$. As illustrated in Figure 5B, the parallel and perpendicular magnetic components, $M_{//}$ and $M_{\perp}$, correspond to the FM and AFM components of the system. The disparity between the FM and AFM peaks is indicative of a weak canting magnetic moment, with AFM dominant in regions of weak magnetic field. With the progressive strengthening of the magnetic field, the spin magnetic moment of the canting structure rotates toward the applied magnetic field direction, leading to a gradual increase in the FM component and a concomitant expansion in the lattice constant. Figure 5C illustrates the magnetic field dependence of the lattice constant in $La(Fe,Al)_{13}$. It is noteworthy that the lattice constant displays an increasing trend with increasing magnetic field strength. Of particular significance is the observation that at a temperature of 100 K under a magnetic field of 5 T, $La(Fe,Al)_{13}$ exhibits a large lattice parameter change of 0.25%, which is consistent with prior macroscopic strain measurements conducted in other studies. Additionally, macroscopic magnetic measurements indicate that $La(Fe,Al)_{13}$ materials manifest metamagnetic transitions proximal to a temperature of 100 K, providing valuable insights into the multifaceted magnetic behaviors exhibited by this material system [Figure 5D].

The $La(Fe,Si/Al)_{13}$-based materials showcase notable magnetostriction, surpassing the magnetostriction of $TbFe_2$-based compounds (0.11%) which are renowned for their extensive magnetostriction[41]. Notably, the magnetostriction exhibited by the $La(Fe,Si/Al)_{13}$-based materials demonstrates an exceptional isotropic nature, a distinctive characteristic rarely observed among other magnetostriction materials. The

unprecedented magnetostriction of the La(Fe,Si/Al)$_{13}$-based materials shed light on its potential applications in various scientific and engineering domains.

Magnetocaloric effects in LaFe$_{13}$-based compounds

Solid-state caloric effect refers to the alteration in entropy or temperature within a field, such as a magnetic field, stress, hydrostatic pressure, or electric field. Materials exhibiting solid-state caloric phenomena hold significant promise for advancing the development of environmentally friendly and efficient alternatives to conventional vapor-compression-based cooling devices[42-44]. The IEM transition of La(Fe,Si/Al)$_{13}$-based materials induces a notable change in entropy. Due to the coupling of spin and lattice, these magnetic phase transitions occur not only during temperature changes but also under the influence of an external magnetic field. Specifically, when exposed to a magnetic field, the LaFe$_{13-x}$Si$_x$ undergoes a transformation from a PM state to an FM state, while LaFe$_{13-x}$Al$_x$ experiences a transformation from either a PM state or an AFM state to an FM state. These transitions are accompanied by magnetic entropy change and lattice entropy change. As a result, these materials exhibit a considerable MCE near the magnetic transition temperature, offering potential applications in magnetic cooling technologies.

In 2000, Hu *et al.* presented a pioneering study on the MCE in LaFe$_{13-x}$Al$_x$-based materials[45,46]. They made a novel discovery that the incorporation of a minor quantity of Co atoms has dual effects. Firstly, it causes the T_C of the material to rise due to the changing distribution of electrons, which is closely related to the operating temperature of magnetic refrigeration. Secondly, it induces a transition of the magnetic ground state in LaFe$_{13-x}$Al$_x$, transforming it from an AFM state to an FM state[45,46]. As previously discussed, LaFe$_{13-x}$Al$_x$-based materials display AFM ground states when x is less than 1.7. Intriguingly, the substitution of Fe atoms with a small proportion of Co atoms in LaFe$_{11.12}$Co$_{0.71}$Al$_{1.17}$ results in a transition to an FM ground state characterized by a T_C of 280 K. Furthermore, this transition is accompanied by a peak ΔS_M of 9.1 J kg^{-1} K^{-1} under a 5 T magnetic field, highlighting the potential of LaFe$_{13}$-based materials for magnetocaloric applications.

Figure 6A illustrates the temperature dependence of the entropy change and temperature change of LaFe$_{13-x}$Si$_x$, revealing an intriguing trend in its magnetic refrigeration operating temperature with varying Si content[47]. Specifically, increasing the Si content results in a reduced distance between Fe atoms and a change in the electronic structure, leading to a stronger magnetic exchange interaction, and the magnetic refrigeration operating temperature gradually rises. However, a reduction in the number of Fe atoms results in decreased magnetization, with the peak value of the magnetic entropy change gradually reducing. The peak values of magnetic entropy and temperature change are 30 J kg^{-1} K^{-1} and 12 K under the influence of a 5 T magnetic field when x = 1.3, corresponding to an approximate T_C of 185 K. In contrast, as x reduces to 2.08, the peak magnetic entropy and temperature change diminishes to 10 J kg^{-1} K^{-1} and 5 K under a 5 T magnetic field with an increased operating temperature to approximately 235 K. Furthermore, the peak value of magnetic entropy change reaches 32 J kg^{-1} K^{-1} under a 7 T magnetic field in LaFe$_{11.6}$Si$_{1.4}$, which indicates that the magnetic field of 5 T is sufficient to saturate the MCE of La(Fe,Si)$_{13}$ [Figure 6B][48]. Nevertheless, despite the utilization of Si content manipulation as a means to regulate the magnetic refrigeration working temperature, it becomes evident that this approach alone falls short of achieving room temperature magnetic cooling. Furthermore, the substantial weakening of the magnetic entropy change further underscores the challenges in achieving high temperature ranges for magnetic cooling applications.

In order to enhance the regulation of the magnetic entropy change of La(Fe,Si/Al)$_{13}$-based materials, two distinct methodologies, hydrogenation and Co-substitution of Fe, have been developed. Hydrogenation involves the insertion of H atoms into the atomic gap of La(Fe,Si/Al)$_{13}$-based materials under high-pressure

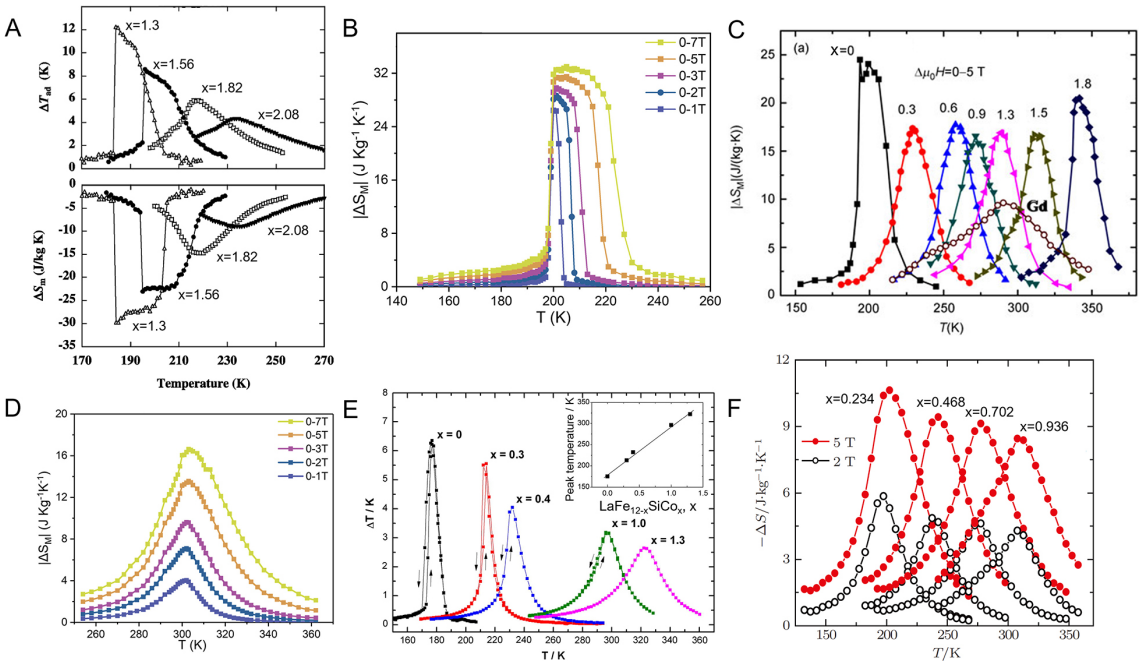

Figure 6. (A) Temperature dependence of the isothermal magnetic entropy change and adiabatic temperature change for $LaFe_{13-x}Si_x$ with x = 2.08, 1.82, 1.56, and 1.3 in the magnetic field changes from 0 to 5 T[47]. (B) Isothermal magnetic entropy changes for $LaFe_{11.6}Si_{1.4}$[48]. (C) Temperature dependence of the isothermal magnetic extropy change for $LaFe_{11.5}Si_{1.5}H_x$[49]. (D) Isothermal magnetic entropy changes for $LaFe_{10.6}Co_1Si_{1.4}$[48]. (E) Temperature dependence of the isothermal magnetic entropy change for $LaFe_{11.5}Si_{1.5}H_x$ with x = 0, 0.3, 0.6, 0.9, 1.3, 1.5, and 1.8[50]. (F) Temperature dependence of the isothermal magnetic extropy change for $LaFe_{11.7-x}Co_xAl_{1.3}$[17]. (A) is reproduced with the permission of Ref.[47] Copyright 2003, Taylor&Francis Group. (B and D) are reproduced with the permission of Ref.[48] Copyright 2023, Elsevier. (C) is reproduced with the permission of Ref.[49] Copyright 2013, Springer Nature. (E) is reproduced with the permission of Ref.[50] Copyright 2012, Elsevier. (F) is reproduced with the permission of Ref.[17] Copyright 2013, Editorial Office of Chinese Physics B.

conditions. Figure 6C illustrates the temperature dependence of magnetic entropy change for $LaFe_{11.5}Si_{1.5}H_x$, showcasing the impact of H-atom insertion x on the magnetic cooling operating and the magnitude of the magnetic entropy change. Remarkably, the magnetic refrigeration operating temperature gradually rises with increasing x while the magnetic entropy change maintains a substantial magnitude attributable to the preservation of the first-order magnetic transition[49]. When the H-atom insertion x reaches 1.3 or 1.5, the magnetic refrigeration operating temperature of $LaFe_{11.5}Si_{1.5}H_x$ approaches room temperature while the peak value of the magnetic entropy change remains at 16 J kg^{-1} K^{-1}, which fulfills the demand for room-temperature refrigeration. In addition, the magnetic entropy change of Gd, a well-known magnetic refrigeration material, depicted in Figure 6C, reveals that $LaFe_{11.5}Si_{1.5}H_{1.3}$ exhibits significantly stronger magnetic entropy change magnitude than Gd (9.7 J kg^{-1} K^{-1}, T_C = 293 K). This comparison shows the exceptional effectiveness of hydrogenation as a method to increase the magnitude of the magnetic entropy change in $La(Fe,Si/Al)_{13}$-based materials.

The substitution of Fe atoms with Co atoms constitutes a well-established approach for modulating the magnetic entropy change in $La(Fe,Si/Al)_{13}$-based materials. The incorporation of Co atoms influences not only the lattice constant but also the electronic states within the material, thereby imparting a significant impact on its magnetic properties. As illustrated in Figure 6D, an analysis of the temperature dependence of magnetic entropy change in $LaFe_{10.6}Co_{1.0}Si_{1.4}$ reveals that the substitution of Fe atoms with Co atoms leads to a significant expansion of the temperature range over which magnetic entropy changes manifest. A remarkable peak value of entropy change of 17 J kg^{-1} K^{-1} is achieved under a 7 T magnetic field at 300 K[48].

According to the temperature dependence of adiabatic temperature change of $LaFe_{12-x}Co_xSi$, the substitution of Co atoms results in a substantial elevation of the operational temperature for magnetic refrigeration, although the temperature changes and cooling capacity are reduced [Figure 6E][50]. Figure 6F illustrates the temperature dependence of the magnetic entropy change for $LaFe_{11.7-x}Co_xAl_{1.3}$. Comparatively, the magnetic entropy change for $LaFe_{13-x}Al_x$ is generally lower than that for $LaFe_{13-x}Si_x$ due to its weaker magnetic properties. However, the introduction of a small amount of Co atoms yields a substantial increase in the magnetic cooling operating temperature while maintaining the magnetic entropy change within a considerable range. Specifically, $LaFe_{10.764}Co_{0.963}Al_{1.3}$ exhibits a peak magnetic entropy change of 8.5 J kg^{-1} K^{-1} corresponding to a temperature of 309 K under a 5 T magnetic field[17].

Through the above comparison, it becomes evident that both hydrogenation and substitution of Co for Fe atoms are effective means to increase the magnetic entropy change temperature of $La(Fe,Si/Al)_{13}$-based materials to room temperature. However, the hydrogenation process presents challenges, given the requirement for sophisticated equipment, intricate procedures, difficulty in controlling the number of H atoms during hydrogenation, and the tendency of H atoms to detach from the material after hydrogenation. Mayer *et al.* have developed a novel process based on gas atomization and powder metallurgy techniques to produce stable $LaFe_{13}H_x$-based materials, setting the stage for the development of advanced magnetic refrigeration equipment using $LaFe_{13}H_x$-based materials[51]. On the other hand, the Co-substitution method offers practical advantages, as only a tiny quantity of Co atoms needs to be introduced during the melting process, and precise control over the Co atom content is achievable. Therefore, the Co-substitution method proves superior in controlling the temperature of magnetic entropy change, providing a viable and effective approach for practical applications.

As mentioned above, the substitution of Co atoms with a smaller atomic radius than Fe atoms has been found to achieve an increase in the MCE temperature. Conversely, employing Cr atoms with a larger atomic radius than Fe atoms leads to a contrasting effect, attributed to the weaker magnetism and reduced number of valence electrons. The magnetic refrigeration temperature of $LaFe_{11.6-x}Cr_xSi_{1.4}$ exhibits a gradual decrease concomitant with an increase in the Cr content, resulting in commensurate reductions in both the peak magnetic entropy change and adiabatic temperature change. For instance, the operational temperature of magnetic refrigeration reduces from 190 to 173 K when the Cr content reaches x = 0.56. Additionally, the peak value of entropy change experiences a corresponding drop from 23 to 7 J kg^{-1} K^{-1} [Figure 7A][52]. The substitution of Ni and Cr atoms leads to reductions in entropy change and adiabatic temperature change. In particular, Ni atom substitution instigates a more pronounced reduction in the MCE (Inset of Figure 7A).

Dong *et al.* conducted an investigation on the MCE of $LaFe_{11.4}Al_{1.6-x}Si_x$ (x = 0.3, 0.8) [Figure 7B and C][53]. The low-temperature magnetic ground state exhibits FM characteristics in $LaFe_{11.4}Al_{1.3}Si_{0.3}$. However, it undergoes a transformation to AFM at T_0 = 135 K and PM at T_N = 188 K. Consequently, the temperature dependence of magnetic entropy change manifests two peaks, corresponding to the magnetic transitions from FM to AFM and from AFM to PM, respectively. It is essential to note that a prominent peak of 29 J kg^{-1} K^{-1} appears at 135 K, resulting from an artifact brought about by Maxwell relation calculations[54,55]. Therefore, the magnetic entropy change curve of $LaFe_{11.4}Al_{1.3}Si_{0.3}$ exhibits a wide temperature plateau ranging from 130 to 210 K, with the maximum peak of the magnetic entropy change measuring 8 J kg^{-1} K^{-1} under a magnetic field of 5 T. For $LaFe_{11.4}Al_{0.8}Si_{0.8}$, an FM state is observed at low temperature, which undergoes a transition to a PM state at T_C = 185 K. The temperature dependence of magnetic entropy change displays a single peak, corresponding to the FM-PM transition. The magnitude of the peak is 14 J kg^{-1} K^{-1} under a magnetic field of 5 T[53]. Shen *et al.* conducted a thorough investigation on the MCE of $LaFe_{11.03}Co_{0.8}Al_{1.17-x}Si_x$, leading to the notable observation that the T_C of the material exhibits a decreasing trend with increasing Si

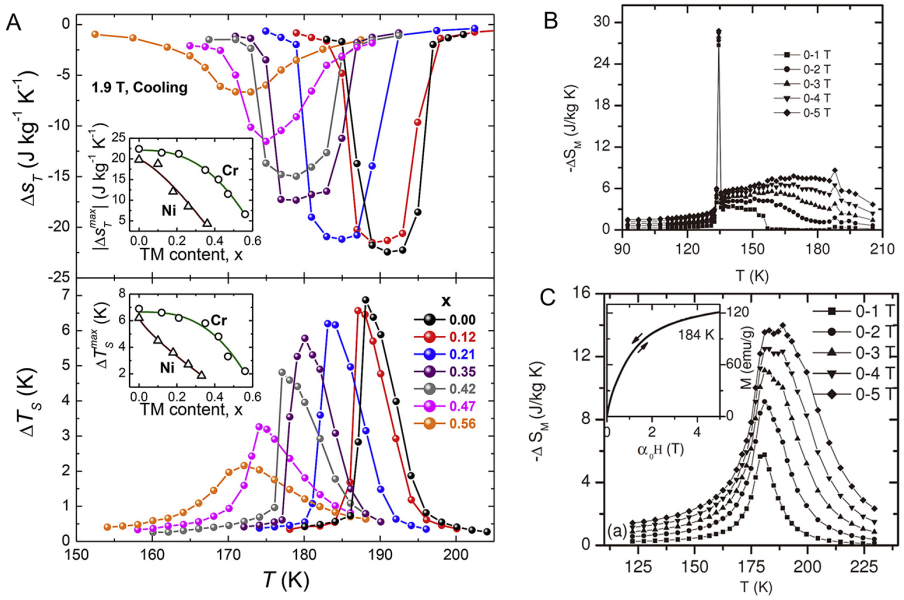

Figure 7. (A) Temperature dependence of isothermal magnetic entropy change and adiabatic temperature change for $LaFe_{11.6-x}Cr_xSi_{1.4}$. Insets display the peak values of isothermal magnetic entropy change and adiabatic temperature change as a function of the Cr content, compared to Ni-doped data[52]. (B and C) Temperature dependence of the isothermal magnetic entropy change for $LaFe_{11.4}Al_{1.3}Si_{0.3}$ and $LaFe_{11.4}Al_{0.8}Si_{0.8}$[53]. (A) is reproduced with the permission of Ref.[52] Copyright 2019, Elsevier. (B and C) are reproduced with the permission of Ref.[53] Copyright 2008, IOP Publishing.

content [Figure 8][17]. Moreover, the addition of Si atoms gradually enhances the peak magnitude of the magnetic entropy change. A direct comparison between $LaFe_{11.03}Co_{0.8}Al_{0.7}Si_{0.47}$ and $LaFe_{11.03}Co_{0.8}Si_{1.17}$ under a 5 T magnetic field reveals an increase in the peak magnitude of the magnetic entropy change from 8.8 to 18.5 J kg^{-1} K^{-1}, accompanied by a reduction in the half-height width from 55 to 28 K[17]. These findings signify more pronounced first-order magnetic transition characteristics with the rise in Si content. Consequently, the characteristics of the IEM transition are augmented. On the basis of these results, it can be concluded that the rise in Al content in $La(Fe,Co,Al,Si)_{13}$ materials significantly influences the magnetic exchange interactions between magnetic atoms. The incorporation of Al atoms introduces the AFM phase into the materials, thereby suppressing the magnitude of the magnetic entropy change of $La(Fe,Co,Al,Si)_{13}$. Nonetheless, this also leads to the broadening of the temperature range of magnetic refrigeration, attributed to the appearance of two distinct peaks in the magnetic entropy transition. In addition, the substitution of Co atoms influences both the lattice and electron concentration, which increases the T_C of $LaFe_{13}$-based materials significantly.

The operational principle of magnetic refrigeration equipment is shown in Figure 9A. Loading a magnetic field causes $La(Fe,Si)_{13}$ to transition from a PM state to an FM state, resulting in volume expansion and heat release. Conversely, the removal of the magnetic field prompts an inverse process, leading to volume shrinkage and heat absorption. The contribution compounded by the combined influences of magnetic entropy change and lattice entropy change endows $La(Fe,Si)_{13}$ with its distinctive and noteworthy characteristics as a magnetic refrigeration material. In an effort to explore the impact of multiple fields on the MCE of $La(Fe,Si)_{13}$, Lyubina *et al.* conducted a comprehensive investigation on the MCE of $LaFe_{11.57}Si_{1.43}$ and $LaFe_{11.57}Si_{1.43}H_{1.64}$ under pressure [Figure 9B and C][56]. The T_C of $LaFe_{11.57}Si_{1.43}$ at atmospheric pressure measures 202 K, with the peak magnetic entropy change reaching 150 kJ/m^3 K under a 5 T magnetic field. Due to the volume of the PM state being smaller than that of the FM state, the external hydrostatic pressure field is more favorable to the stability of the PM state. The T_C gradually decreases upon application of

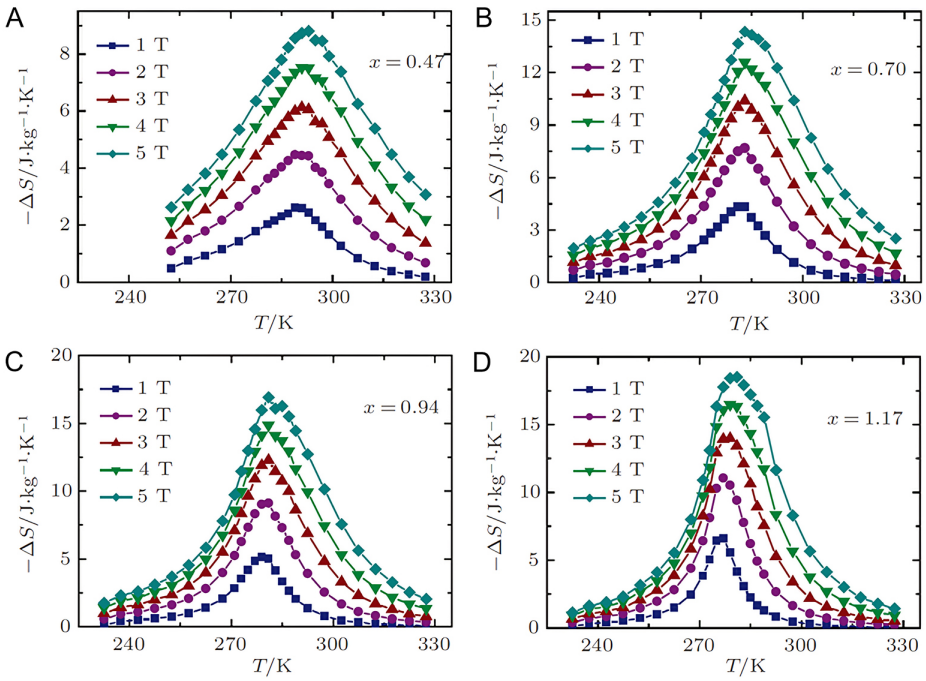

Figure 8. Temperature dependence of the isothermal magnetic entropy change for $LaFe_{11.03}Co_{0.8}Al_{1.17-x}Si_x$ [x = (A) 0.47, (B) 0.70, (C) 0.94, (D) 1.17] for different magnetic field changes[17]. (A-D) are reproduced with the permission of Ref.[17] Copyright 2013, Editorial Office of Chinese Physics B.

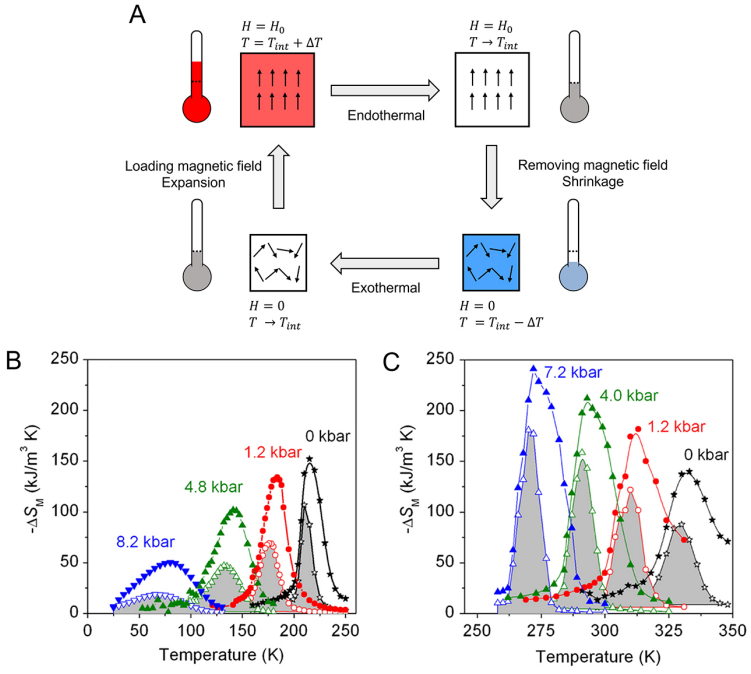

Figure 9. (A) The operational principle of magnetic refrigeration equipment. (B and C) Temperature and pressure dependence of the isothermal magnetic entropy change in $LaFe_{11.57}Si_{1.43}$ and $LaFe_{11.57}Si_{1.43}H_{1.64}$. Open and closed symbols correspond to magnetic entropy change for a field change of 2 and 5 T, respectively[56]. (B and C) are reproduced with the permission of Ref.[56] Copyright 2008, American Physical Society.

hydrostatic pressure, leading to a corresponding decrease in the peak value of the magnetic entropy change. At a hydrostatic pressure of 8.2 kbar, the peak magnetic entropy change in $LaFe_{11.57}Si_{1.43}$ decreases to 50 kJ/m^3 K. For $LaFe_{11.57}Si_{1.43}H_{1.64}$, the insertion of H increases the T_C to 329 K, with only a slightly decrease observed in the peak magnetic entropy change. Similar to $LaFe_{11.57}Si_{1.43}$, the T_C of $LaFe_{11.57}Si_{1.43}H_{1.64}$ also decreases with increasing hydrostatic pressure. However, a notable observation is the significant enhancement in the peak of the magnetic entropy change for $LaFe_{11.57}Si_{1.43}H_{1.64}$ with increasing hydrostatic pressure. The peak magnetic entropy change reaches 248 kJ/m^3 K when the hydrostatic pressure reaches 7.2 kbar[56]. Analyses of the half-height width of the magnetic entropy change for both materials reveal intriguing phenomena. Specifically, $LaFe_{11.57}Si_{1.43}$ shifts from a first-order transition to a second-order transition under hydrostatic pressure, while the significant enhancement of the characteristics of the first-order phase transition was observed in $LaFe_{11.57}Si_{1.43}H_{1.64}$. The significant enhancement in the magnetic entropy change results from the combined effect of H insertion and the applied hydrostatic pressure. The incorporation of H atoms yields a pronounced impact on the T_C and lattice parameters of $LaFe_{11.57}Si_{1.43}$. Remarkably, $LaFe_{11.57}Si_{1.43}H_{1.64}$ undergoes a first-order phase transition when subjected to hydrostatic pressure, concomitant with a substantial amplification in the magnitude of magnetic entropy variation.

$La(Fe,Si/Al)_{13}$-based materials demonstrate exceptional characteristics as magnetic refrigeration materials, prominently featuring giant magnetic entropy changes that render them highly promising for the development of efficient magnetic refrigeration devices. The comprehensive analyses provided herein underscore the significance of Co-substitution and hydrogenation as effective means to amplify the magnetic entropy change in $La(Fe,Si/Al)_{13}$-based materials, thus fostering new prospects in advanced magnetic refrigeration technologies. Furthermore, the advantageous composition of $La(Fe,Si/Al)_{13}$-based materials, with a predominant iron content and only a minor presence of rare-earth lanthanum, positions them as low-cost materials in addition to their superior magnetic properties.

Barocaloric effects in $LaFe_{13}$-based compounds

Hydrostatic pressure is a significant and effective means of activating solid-state refrigeration materials. The application of hydrostatic pressure leads to the compression of the lattice, resulting in lattice entropy change and magnetic entropy change within magnetic materials. The hydrostatic pressure-driven caloric effect is known as the BCE[57]. In contrast to other solid-state refrigeration techniques (magnetocaloric, elastocaloric, and electrocaloric effects are only present in FM, ferroelectric, and ferroelastic materials), a notable advantage of hydrostatic pressure lies in its direct impact on the lattice, making the BCE pervasive in phase-transition materials. Various materials have demonstrated the BCE, including the ionic conductor AgI, natural rubber, the antiferromagnet Mn_3GaN, the ferrielectric ammonium sulfate, and plastic crystals[58-63]. In $La(Fe,Si)_{13}$-based materials, hydrostatic pressure compresses the atomic distance in the crystal and alters the magnetic exchange interactions in the system. It is important to note that the volume of the FM state in $La(Fe,Si)_{13}$-based materials is larger than that of the PM state. Unlike "chemical pressure" obtained via interstitial atom insertion or alternative approaches, the "physical pressure" of hydrostatic pressure plays a critical role in the FM state transitions to the PM state because of the strong spin-lattice coupling [Figure 10][64]. This phenomenon contributes to the emergence of a remarkable BCE in $La(Fe,Si)_{13}$-based materials.

Mañosa *et al.* studied the BCE in $LaFe_{11.33}Co_{0.47}Si_{1.2}$. The temperature dependence of entropy variation in $LaFe_{11.33}Co_{0.47}Si_{1.2}$ indicates that the entropy increases by 11.4 J kg^{-1} K^{-1} during the warming process [Figure 11A][65]. This entropy change is distinctly associated with the FM to PM phase transition, which exhibits a gradual shift to lower temperatures under increasing hydrostatic pressure. Figure 11B illustrates the temperature dependence of entropy change in $LaFe_{11.33}Co_{0.47}Si_{1.2}$, calculated as $\Delta S(T, P) = S(T, P) - S(T, 0)$. Notably, the magnitude of the isothermal entropy change progressively increases with rising

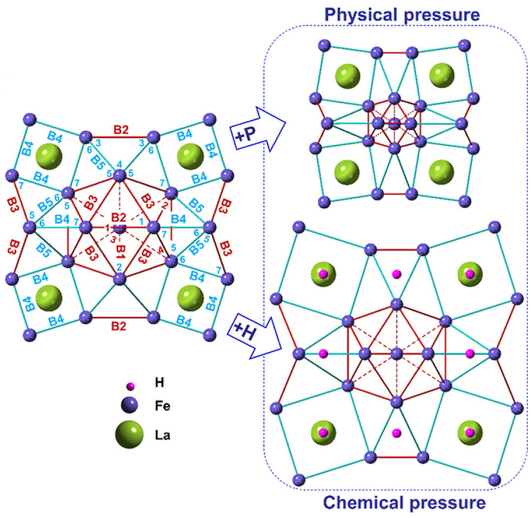

Figure 10. Diagram depicting modifications in the local atomic environment induced by physical or chemical pressure[64]. Reproduced with the permission of Ref.[64] Copyright 2020, American Chemical Society.

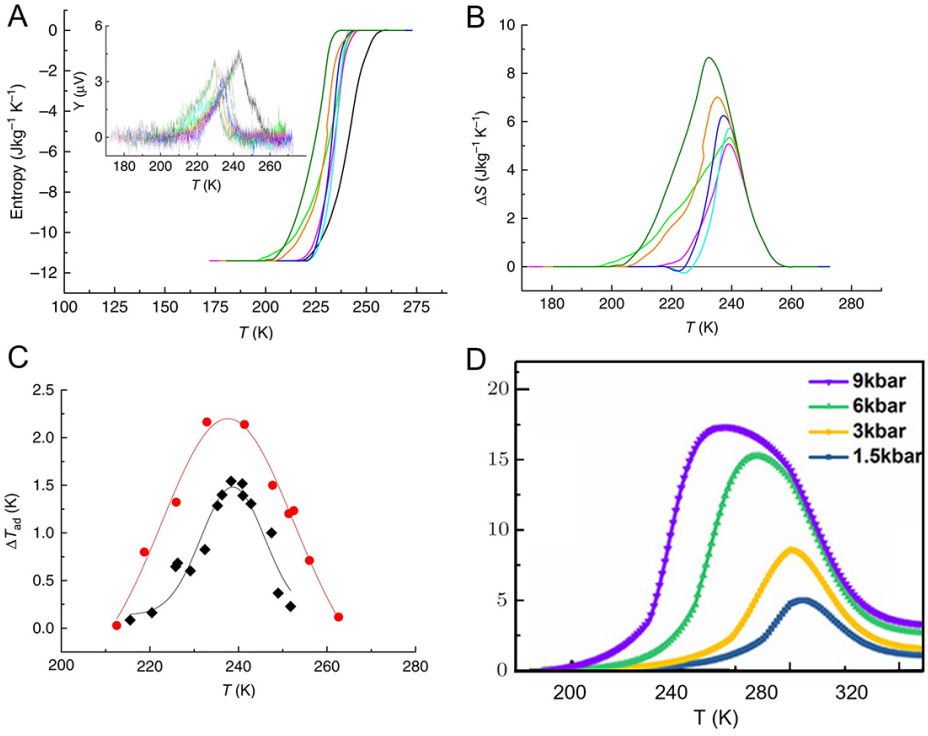

Figure 11. Temperature dependence of (A) isothermal entropy change (B) entropy in $LaFe_{11.33}Co_{0.47}Si_{1.2}$ [65]. The black line corresponds to 0 kbar; green: 0.8 kbar; magenta: 1 kbar; cyan: 1.2 kbar; blue: 1.4 kbar; orange: 1.7 kbar; olive: 2.1 kbar [65]. (C) Temperature dependence of adiabatic temperature change on fast release of hydrostatic pressure. Diamonds correspond to 1 kbar and circles to 2 kbar (lines are guides to the eye) [65]. (D) Temperature dependence of entropy change corresponds to different hydrostatic pressures[64]. (A-C) are reproduced with the permission of Ref.[65] Copyright 2011, Springer Nature. (D) is reproduced with the permission of Ref.[64] Copyright 2020, American Chemical Society.

pressure, culminating in a peak value of 8.6 J kg^{-1} K^{-1} below T_C = 250 K at a pressure of 2.1 kbar. This observation indicates that a higher pressure is required to reach the maximum value of 11.4 J kg^{-1} K^{-1} for the

theoretical entropy change. Although the isothermal entropy change is vital for evaluating the cooling capacity of materials, it is equally important to ascertain the magnitude of the adiabatic temperature change in practical applications. Figure 11C demonstrates the temperature dependence of adiabatic temperature change in $LaFe_{11.33}Co_{0.47}Si_{1.2}$ measured directly upon instantaneously withdrawing pressure from 1 kbar (black diamond) and 2 kbar (red circles) hydrostatic conditions, yielding peak values of 1.5 and 2.2 K, respectively[65]. Figure 11D shows the BCE in $LaFe_{10.948}Co_{0.952}Si_{1.1}$ studied by Hao *et al.* The peak magnitude of the BCE reaches 17.4 J kg^{-1} K^{-1} at a hydrostatic pressure of 9 kbar[64]. The difference in entropy change between $LaFe_{10.948}Co_{0.952}Si_{1.1}$ and $LaFe_{11.33}Co_{0.47}Si_{1.2}$ can be attributed to variations in Co-atom and Si-atom contents, alongside the magnitude of hydrostatic pressure. The magnitude of the isothermal entropy change in the BCE is proportionate to the volume change before and after the phase transition. After normalization using the volume change amounts of both materials, the entropy change results of the BCE demonstrate remarkable consistency.

Given the significance of a substantial BCE and a notable adiabatic temperature change under low pressure in practical applications, Liu *et al.* designed a material $La_{1.2}Ce_{0.8}Fe_{11}Si_2H_{1.86}$ with a hydride of $La(Fe,Si)_{13}$ in the main phase[66]. In this material, the rate of change of the T_C with respect to pressure (dT_C/dP) is approximately -26 K $kbar^{-1}$, surpassing that of existing metallic barocaloric materials. This enhanced sensitivity of T_C to hydrostatic pressure not only facilitates a reduction in the required driving pressure for BCE but also contributes to an improved adiabatic temperature change. Figure 12A illustrates the temperature dependence of the adiabatic temperature change, calculated using the "Transition distribution model" for $La_{1.2}Ce_{0.8}Fe_{11}Si_2H_{1.86}$, which reaches 8 and 11 K at hydrostatic pressures of 1 and 1.4 kbar, respectively. These results are consistent with the indirect measurements obtained by differential scanning calorimetry (DSC). Figure 12B demonstrates the time dependence of adiabatic temperature change measured directly in $La_{1.2}Ce_{0.8}Fe_{11}Si_2H_{1.86}$. The temperature of the sample decreases gradually when loading hydrostatic pressure. When T = 290 K and a 1 kbar hydrostatic pressure was instantaneously loaded, the temperature of the sample decreased to 282 K within 50 s, which represented ΔT_{BCE} = 8 K for the sample. The temperature of the sample remains almost constant for 70 s while maintaining the pressure. The temperature of the sample gradually returned to the initial value upon momentarily withdrawing the hydrostatic pressure. The experimental findings underscore the presence of a substantial adiabatic temperature change under low pressure in $La_{1.2}Ce_{0.8}Fe_{11}Si_2H_{1.86}$, thereby affirming its potential for practical application in solid-state refrigeration technologies. To obtain insight into the physical mechanism of BCE in $La_{1.2}Ce_{0.8}Fe_{11}Si_2H_{1.86}$, neutron scattering measurements were carried out as a function of temperature, magnetic field, and hydrostatic pressure [Figure 12C]. The resulting lattice constants obtained via neutron diffraction data indicate a magnetic-field-induced volume change of 1.6% at 280 K in $La_{1.2}Ce_{0.8}Fe_{11}Si_2H_{1.86}$ [Figure 12D]. However, it is noteworthy that the volume of $La_{1.2}Ce_{0.8}Fe_{11}Si_2H_{1.86}$ contracted by a comparatively lesser magnitude of 1.2% during the heating process, a phenomenon reasonably attributed to the thermal expansion exhibited by the crystalline lattice as a consequence of the warming process [Figure 12E]. Furthermore, a hydrostatic pressure of 6.3 kbar serves to contract the volume of $La_{1.2}Ce_{0.8}Fe_{11}Si_2H_{1.86}$ by 2% at 280 K, resulting from the combined effects of MCE and pressure-induced effects [Figure 12F][66]. Results of lattice constant obtained under varying external fields provide evidence of strong coupling between the spin and lattice in $La_{1.2}Ce_{0.8}Fe_{11}Si_2H_{1.86}$. These findings also highlight the collective impact of the magnetic structure and crystal structure phase transition, resulting in the giant BCE observed in the material.

The BCE has emerged as a highly captivating research area in recent years, garnering substantial interest among researchers. Notably, $La(Fe,Si)_{13}$-based materials exhibit remarkable BCE. Leveraging the potential of elemental substitution and hydrogenation, the BCE in these materials can be finely tuned, leading to

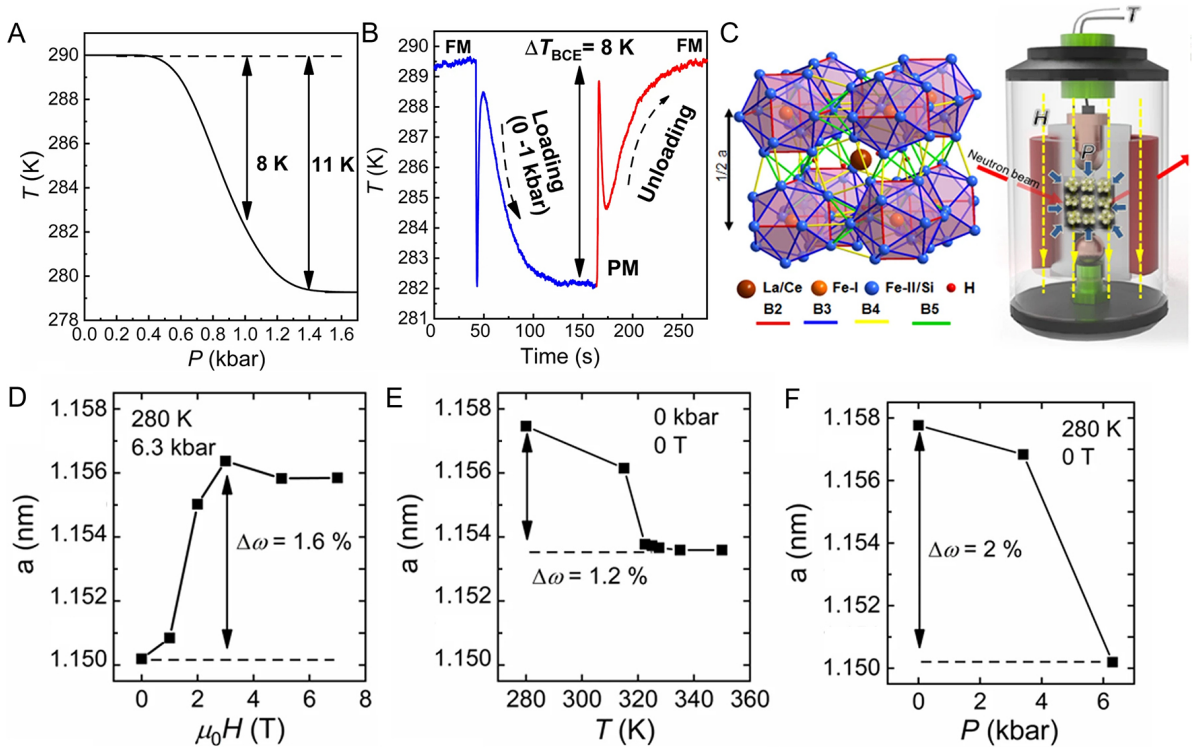

Figure 12. (A) Pressure dependence of calculated adiabatic temperature by the transition distribution model[66]. (B) Directly measured time-dependent adiabatic temperature curve under a pressure of 1 kbar at 289.5 K[66]. (C) Schematic diagram of La-Ce-Fe-Si-H crystal structure and in situ neutron diffraction device[66]. Lattice parameters as a function of (D) hydrostatic pressure, (E) magnetic field, and (F) temperature, respectively[66]. (A-F) are reproduced with the permission of Ref.[66] Copyright 2022, Springer Nature.

substantial adiabatic temperature variations under low-pressure conditions. Furthermore, the operating temperature of the BCE can be flexibly adjusted, offering promising prospects for practical applications of this class of materials in diverse fields. By overcoming the problems of low entropy change and refrigeration efficiency, more efficient refrigeration equipment can be developed. The adaptability and exceptional performance of $La(Fe,Si)_{13}$-based materials underscore their significant application potential in solid-state refrigeration technologies. Efforts moving forward are expected to concentrate on developing innovative refrigeration equipment with optimized heat transfer efficiency.

CONCLUSIONS AND PERSPECTIVES

Magnetic functional materials have not only become the focus of fundamental research but also have found extensive applications in contemporary society. This comprehensive review encompasses an array of investigations into $La(Fe,Si/Al)_{13}$-based materials, shedding light on their promising magnetic functionalities caused by coupling between spin and lattice. The variation in volume across distinct magnetic structures serves as the cornerstone, with the robust spin-lattice coupling emerging as a pivotal determinant of the functionalities exhibited by $LaFe_{13}$-based materials. External fields assume a pivotal role as driving forces in the induction of desired functionalities within these materials. Elevating the temperature or applying hydrostatic pressure triggers a phase transition, transitioning from a large to a small volume state, thereby showcasing giant NTE and BCE in $LaFe_{13}$-based materials. In contrast, the application of a magnetic field can effectuate a transformation from a small to a large volume phase, concurrently eliciting giant magnetostriction and MCE [Figure 13]. The capability to manipulate the functionalities of $LaFe_{13}$-based materials through diverse physical fields endows them with the potential to function as smart materials[67-70].

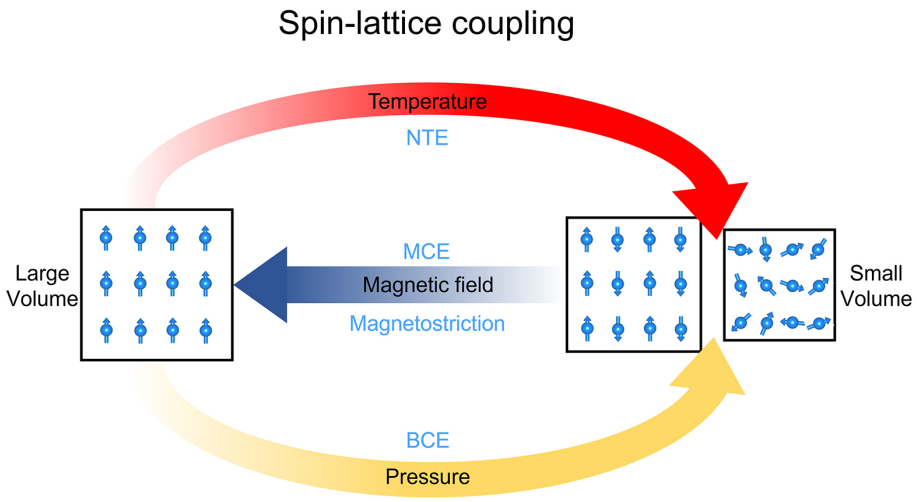

Figure 13. The relationship between spin-lattice coupling and exceptional magnetic functionalities.

Moreover, it delves into the roles of the IEM transition, providing valuable insights into magnetic effects. The modulation of magnetic functionalities in La(Fe,Si/Al)$_{13}$-based materials can be achieved through diverse means, including elemental substitution, hydrogenation, and the application of the external field. These methods effectively alter the coupling between spin and lattice by influencing the lattice structure, electronic structures, and magnetic properties.

La(Fe,Si/Al)$_{13}$-based materials exhibit giant NTE over a wide temperature range. The NTE in La(Fe,Si/Al)$_{13}$-based materials is induced by the coupling of spin and lattice at FM-PM or AFM-PM transitions. By controlling magnetic transition through chemical substitution or hydrogenation, the operational temperature range of NTE can be controlled to encompass room temperature. In La(Fe,Si)$_{13}$-based materials, a 1% magnetostriction of unit-cell volume occurs above T_C during the IEM transition from PM to FM upon loading the magnetic field. A large isotropic magnetostriction of 0.25% along the magnetic field below T_N can be achieved with the IEM transition from AFM to FM with a magnetic field of 5 T in La(Fe,Al)$_{13}$-based materials. These materials have also demonstrated outstanding MCE and BCE during the IEM transition under the influence of magnetic fields or hydrostatic pressures, thereby establishing them as highly promising candidates for magnetic or pressure-cooling devices. However, despite the progress made so far, there remain challenges to overcome in terms of the mechanical properties and thermal conductivity of LaFe$_{13}$-based materials as intermetallic compounds in industrial applications. Therefore, future research should focus on addressing these issues and exploring the development of magnetostrictive devices and the integration of refrigeration equipment.

La(Fe,Si)$_{13}$-based materials, as a remarkable class of magnetic functional materials, have been thoroughly documented in relevant research. However, further explorations into the mechanism underlying the IEM transition and the interplay between magnetism and structure are desired. Such endeavors will not only lead to advancements in the properties of La(Fe,Si/Al)$_{13}$-based materials but will also promote the development of other categories of magnetic functional materials. Additionally, focused efforts to advance practical applications for La(Fe,Si/Al)$_{13}$-based composite materials hold immense potential for realizing their real-world utility.

DECLARATIONS

Authors' contributions

Supervision, conceptualization, validation, project administration, funding acquisition: Chen J, Song Y
Original draft preparation, reviewing, and editing: Long F, Song Y, Chen J

Availability of data and materials

Not applicable.

Financial support and sponsorship

This work was supported by the National Key Research and Development Program of China (2022YFE0109100), the National Natural Science Foundation of China (22235002, 22275014, and 12104038), the Fundamental Research Funds for the Central Universities, China (06500201), and the Young Elite Scientists Sponsorship Program by CAST.

Conflicts of interest

All authors declared that there are no conflicts of interest.

Ethical approval and consent to participate

Not applicable.

Consent for publication

Not applicable.

REFERENCES

1. Song Y, Shi N, Deng S, Xing X, Chen J. Negative thermal expansion in magnetic materials. *Prog Mater Sci* 2021;121:100835. DOI
2. Song Y, Chen J, Liu X, et al. Zero thermal expansion in magnetic and metallic Tb(Co,Fe)$_2$ intermetallic compounds. *J Am Chem Soc* 2018;140:602-5. DOI
3. Song Y, Xu M, Zheng X, et al. A new method to enhance the magnetocaloric effect in (Sc,Ti)Fe$_2$ via magnetic phase separation. *J Mater Sci Technol* 2023;147:102-11. DOI
4. Stern-Taulats E, Planes A, Lloveras P, et al. Barocaloric and magnetocaloric effects in $Fe_{49}Rh_{51}$. *Phys Rev B* 2014;89:214105. DOI
5. Aznar A, Lloveras P, Kim JY, et al. Giant and reversible inverse barocaloric effects near room temperature in ferromagnetic $MnCoGeB_{0.03}$. *Adv Mater* 2019;31:e1903577. DOI
6. Jungwirth T, Marti X, Wadley P, Wunderlich J. Antiferromagnetic spintronics. *Nat Nanotechnol* 2016;11:231-41. DOI PubMed
7. Awschalom DD, Flatté ME. Challenges for semiconductor spintronics. *Nat Phys* 2007;3:153-9. DOI
8. Palstra TTM, Mydosh JA, Nieuwenhuys GJ, van der Kraan AM, Buschow KHJ. Study of the critical behaviour of the magnetization and electrical resistivity in cubic La(Fe, Si)$_{13}$ compounds. *J Magn Magn Mater* 1983;36:290-6. DOI
9. Palstra TTM, Werij HGC, Nieuwenhuys GJ, Mydosh JA, Boer FRD, Buschow KHJ. Metamagnetic transitions in cubic La(Fe_xAl_{1-x})$_{13}$ intermetallic. *J Phys F Met Phys* 1984;14:1961-6. DOI
10. Yamada H, Inoue J, Shimizu M. Electronic structure and magnetic properties of the cubic Laves phase compounds ACo_2 (A=Sc, Ti, Zr, Lu and Hf) and $ScNi_2$. *J Phys F Met Phys* 1985;15:169-80. DOI
11. Paul-Boncour V, Bessais L. Tuning the magnetocaloric properties of the La(Fe,Si)$_{13}$ compounds by chemical substitution and light element insertion. *Magnetochemistry* 2021;7:13. DOI
12. Liu J, He C, Zhang M, Yan A. A systematic study of the microstructure, phase formation and magnetocaloric properties in off-stoichiometric La-Fe-Si alloys. *Acta Mater* 2016;118:44-53. DOI
13. Niitsu K, Kainuma R. Phase equilibria in the Fe-La-Si ternary system. *Intermetallics* 2012;20:160-9. DOI
14. Raghavan V. Fe-La-Si (iron-lanthanum-silicon). *J Phase Equilib Diff* 2001;22:158-9. DOI
15. Song Y, Huang R, Zhang J, et al. The critical role of spin rotation in the giant magnetostriction of La(Fe,Al)$_{13}$. *Sci China Mater* 2021;64:1238-45. DOI
16. Song Y, Huang R, Liu Y, et al. Magnetic-field-induced strong negative thermal expansion in La(Fe,Al)$_{13}$. *Chem Mater* 2020;32:7535-41. DOI

17. Shen BG, Hu FX, Dong QY, Sun JR. Magnetic properties and magnetocaloric effects in $NaZn_{13}$-type $La(Fe,Al)_{13}$-based compounds. *Chin Phys B* 2013;22:017502. DOI
18. de Medeiros Jr. LG, de Oliveira NA. Magnetocaloric effect in $La(Fe_x,Si_{1-x})_{13}$ doped with hydrogen and under external pressure. *J Alloys Compd* 2006;424:41-5. DOI
19. Li S, Huang R, Zhao Y, Wang W, Han Y, Li L. Zero thermal expansion achieved by an electrolytic hydriding method in $La(Fe,Si)_{13}$ compounds. *Adv Funct Mater* 2017;27:1604195. DOI
20. Rosca M, Balli M, Fruchart D, et al. Neutron diffraction study of $LaFe_{11.31}Si_{1.69}$ and $LaFe_{11.31}Si_{1.69}H_{1.45}$ compounds. *J Alloys Compd* 2010;490:50-5. DOI
21. Phejar M, Paul-Boncour V, Bessais L. Investigation on structural and magnetocaloric properties of $LaFe_{13-x}Si_x(H,C)_y$ compounds. *J Solid State Chem* 2016;233:95-102. DOI
22. Niitsu K, Fujieda S, Fujita A, Kainuma R. Microstructure and magnetic properties of as-quenched cubic and tetragonal $La(Fe_{1-x}Si_x)_{13}$ compounds. *J Alloys Compd* 2013;578:220-7. DOI
23. Zhao Y, Huang R, Li S, et al. Effect of cobalt doping on the structural, magnetic and abnormal thermal expansion properties of $NaZn_{13}$-type $La(Fe_{1-x}Co_x)_{11.4}Al_{1.6}$ compounds. *Phys Chem Chem Phys* 2016;18:20276-80. DOI
24. Liu J, Gong Y, Wang J, et al. Realization of zero thermal expansion in $La(Fe,Si)_{13}$-based system with high mechanical stability. *Mater Des* 2018;148:71-7. DOI
25. Li W, Huang R, Wang W, et al. Low-temperature negative thermal expansion property of Mn doped $La(Fe,Si)_{13}$ compounds. *J Alloys Compd* 2015;628:308-10. DOI
26. Yamada H. Metamagnetic transition and susceptibility maximum in an itinerant-electron system. *Phys Rev B Condens Matter* 1993;47:11211-9. DOI
27. Guillaume CE. Recherches sur les aciers au nickel. *J Phys Theor Appl* 1898;7:262-74. DOI
28. Yokoyama T. Thermal expansion of FeNi Invar and zinc-blende CdTe from the view point of local structure. *Microstructures* 2021;1:2021003. DOI
29. Sun Y, Cao Y, Ren Y, et al. Structure, magnetism and low thermal expansion in $Tb_{1-x}Er_xCo_2Mn_y$ intermetallic compounds. *Microstructures* 2023;3:2023028. DOI
30. Zhou H, Liu Y, Huang R, et al. Tunable negative thermal expansion in $La(Fe, Si)_{13}$/resin composites with high mechanical property and long-term cycle stability. *Microstructures* 2022;2:2022018. DOI
31. Huang R, Liu Y, Fan W, et al. Giant negative thermal expansion in $NaZn_{13}$-type $La(Fe, Si, Co)_{13}$ compounds. *J Am Chem Soc* 2013;135:11469-72. DOI
32. Li W, Huang R, Wang W, et al. Abnormal thermal expansion properties of cubic $NaZn_{13}$-type $La(Fe,Al)_{13}$ compounds. *Phys Chem Chem Phys* 2015;17:5556-60. DOI
33. Pang X, Song Y, Shi N, Xu M, Zhou C, Chen J. Design of zero thermal expansion and high thermal conductivity in machinable *x* LFCS/Cu metal matrix composites. *Compos Part B Eng* 2022;238:109883. DOI
34. Hunter D, Osborn W, Wang K, et al. Giant magnetostriction in annealed $Co_{1-x}Fe_x$ thin-films. *Nat Commun* 2011;2:518. DOI
35. Chopra HD, Wuttig M. Non-joulian magnetostriction. *Nature* 2015;521:340-3. DOI PubMed
36. Lee EW. Magnetostriction and magnetomechanical effects. *Rep Prog Phys* 1955;18:184-229. DOI
37. Fujita A, Akamatsu Y, Fukamichi K. Itinerant electron metamagnetic transition in $La(Fe_xSi_{1-x})_{13}$ intermetallic compounds. *J Appl Phys* 1999;85:4756-8. DOI
38. Fujieda S, Fujita A, Fukamichi K, Yamazaki Y, Iijima Y. Giant isotropic magnetostriction of itinerant-electron metamagnetic $La(Fe_{0.88}Si_{0.12})_{13}H_y$ compounds. *Appl Phys Lett* 2001;79:653-5. DOI
39. Ghorbani Zavareh M, Skourski Y, Skokov KP, et al. Direct measurement of the magnetocaloric effect in $La(Fe, Si, Co)_{13}$ compounds in pulsed magnetic fields. *Phys Rev Appl* 2017;8:014037. DOI
40. Abdulkadirova NZ, Gamzatov AG, Kamilov KI, et al. Magnetostriction and magnetocaloric properties of $LaFe_{11.1}Mn_{0.1}Co_{0.7}Si_{1.1}$ alloy: direct and indirect measurements. *J Alloys Compd* 2022;929:167348. DOI
41. Clark AE, Belson HS. Giant room-temperature magnetostrictions in $TbFe_2$ and $DyFe_2$. *Phys Rev B* 1972;5:3642-4. DOI
42. Franco V, Blázquez J, Ipus J, Law J, Moreno-ramírez L, Conde A. Magnetocaloric effect: from materials research to refrigeration devices. *Prog Mater Sci* 2018;93:112-232. DOI
43. Reis MS. Magnetocaloric and barocaloric effects of metal complexes for solid state cooling: review, trends and perspectives. *Coord Chem Rev* 2020;417:213357. DOI
44. Shen BG, Sun JR, Hu FX, Zhang HW, Cheng ZH. Recent progress in exploring magnetocaloric materials. *Adv Mater* 2009;21:4545-64. DOI
45. Hu FX, Shen BG, Sun JR, Cheng ZH, Zhang XX. Magnetic entropy change in $La(Fe_{0.98}Co_{0.02})_{11.7}Al_{1.3}$. *J Phys Condens Matter* 2000;12:L691. DOI
46. Hu FX, Shen BG, Sun JR, Zhang XX. Great magnetic entropy change in $La(Fe, M)_{13}$ (M = Si, Al) with Co doping. *Chin Phys* 2000;9:550. DOI
47. Fujieda S, Fujita A, Fukamichi K. Large magnetocaloric effects in $NaZn_{13}$-type $La(Fe_xSi_{1-x})_{13}$ compounds and their hydrides composed of icosahedral clusters. *Sci Technol Adv Mater* 2003;4:339-46. DOI
48. Zhou HB, Yu ZB, Hu FX, et al. Emergence of Invar effect with excellent mechanical property by electronic structure modulation in $LaFe_{11.6-x}Co_xSi_{1.4}$ magnetocaloric materials. *Acta Mater* 2023;260:119312. DOI

49. Zhang H, Hu FX, Sun JR, Shen BG. Effects of interstitial H and/or C atoms on the magnetic and magnetocaloric properties of La(Fe, Si)$_{13}$-based compounds. *Sci China Phys Mech Astron* 2013;56:2302-11. DOI
50. Löwe K, Liu J, Skokov K, et al. The effect of the thermal decomposition reaction on the mechanical and magnetocaloric properties of La(Fe,Si,Co)$_{13}$. *Acta Mater* 2012;60:4268-76. DOI
51. Mayer C, Dubrez A, Pierronnet M, Vikner P. Towards the large scale production of $(La_{1-z}Ce_z)(Fe_{1-x-y}Mn_ySi_x)_{13}H_n$ products for room temperature refrigeration. *Phys Status Solidi C* 2014;11:1059-63. DOI
52. Moreno-Ramírez LM, Romero-Muñiz C, Law JY, et al. Tunable first order transition in La(Fe,Cr,Si)$_{13}$ compounds: retaining magnetocaloric response despite a magnetic moment reduction. *Acta Mater* 2019;175:406-14. DOI
53. Dong QY, Zhang HW, Sun JR, Shen BG. Effect of Si doping on the magnetic properties and magnetic entropy changes in the $LaFe_{11.4}Al_{1.6}$ intermetallic compound. *J Phys Condens Matter* 2008;20:135205. DOI
54. Zou JD, Shen BG, Gao B, Shen J, Sun JR. The magnetocaloric effect of $LaFe_{11.6}Si_{1.4}$, $La_{0.8}Nd_{0.2}Fe_{11.5}Si_{1.5}$, and $Ni_{43}Mn_{46}Sn_{11}$ compounds in the vicinity of the first-order phase transition. *Adv Mater* 2009;21:693-6. DOI
55. Liu GJ, Sun JR, Shen J, et al. Determination of the entropy changes in the compounds with a first-order magnetic transition. *Appl Phys Lett* 2007;90:032507. DOI
56. Lyubina J, Nenkov K, Schultz L, Gutfleisch O. Multiple metamagnetic transitions in the magnetic refrigerant La(Fe,Si)$_{13}$H$_x$. *Phys Rev Lett* 2008;101:177203. DOI PubMed
57. Mañosa L, Planes A. Materials with giant mechanocaloric effects: cooling by strength. *Adv Mater* 2017;29:1603607. DOI PubMed
58. Carvalho AMG, Imamura W, Usuda EO, Bom NM. Giant room-temperature barocaloric effects in PDMS rubber at low pressures. *Eur Polym J* 2018;99:212-21. DOI
59. Li B, Kawakita Y, Ohira-Kawamura S, et al. Colossal barocaloric effects in plastic crystals. *Nature* 2019;567:506-10. DOI
60. Lloveras P, Aznar A, Barrio M, et al. Colossal barocaloric effects near room temperature in plastic crystals of neopentylglycol. *Nat Commun* 2019;10:1803. DOI PubMed PMC
61. Lloveras P, Stern-Taulats E, Barrio M, et al. Giant barocaloric effects at low pressure in ferrielectric ammonium sulphate. *Nat Commun* 2015;6:8801. DOI PubMed PMC
62. Aznar A, Lloveras P, Romanini M, et al. Giant barocaloric effects over a wide temperature range in superionic conductor AgI. *Nat Commun* 2017;8:1851. DOI PubMed PMC
63. Matsunami D, Fujita A, Takenaka K, Kano M. Giant barocaloric effect enhanced by the frustration of the antiferromagnetic phase in Mn_3GaN. *Nat Mater* 2015;14:73-8. DOI PubMed
64. Hao J, Hu F, Wang JT, et al. Large enhancement of magnetocaloric and barocaloric effects by hydrostatic pressure in $La(Fe_{0.92}Co_{0.08})_{11.9}Si_{1.1}$ with a $NaZn_{13}$-type structure. *Chem Mater* 2020;32:1807-18. DOI
65. Mañosa L, González-Alonso D, Planes A, et al. Inverse barocaloric effect in the giant magnetocaloric La-Fe-Si-Co compound. *Nat Commun* 2011;2:595. DOI
66. Liu Y, Zheng X, Liang F, et al. Large barocaloric effect in intermetallic $La_{1.2}Ce_{0.8}Fe_{11}Si_2H_{1.86}$ materials driven by low pressure. *NPG Asia Mater* 2022;14:30. DOI
67. Li T, Deng S, Qi H, et al. High-temperature ferroic glassy states in $SrTiO_3$-based thin films. *Phys Rev Lett* 2023;131:246801. DOI
68. Gokana MR, Wu CM, Motora KG, Qi JY, Yen WT. Effects of patterned electrode on near infrared light-triggered cesium tungsten bronze/poly(vinylidene)fluoride nanocomposite-based pyroelectric nanogenerator for energy harvesting. *J Power Sources* 2022;536:231524. DOI
69. Rani GM, Ghoreishian SM, Ranjith KS, et al. High roughness induced pearl necklace-like ZIF-67@PAN fiber-based triboelectric nanogenerators for mechanical energy harvesting. *Adv Mater Technol* 2023;8:2300685. DOI
70. Rani GM, Wu CM, Motora KG, Umapathi R, Jose CRM. Acoustic-electric conversion and triboelectric properties of nature-driven CF-CNT based triboelectric nanogenerator for mechanical and sound energy harvesting. *Nano Energy* 2023;108:108211. DOI